Effects of Methylation at the 2 Position of the Cation Ring on Phase Behaviors and Conformational Structures of Imidazolium-Based Ionic Liquids

Takatsugu Endo, Tatsuya Kato, and Keiko Nishikawa*

Graduate School of Advanced Integration Science, Chiba University, 1-33 Yayoi-cho, Inage-ku, Chiba 263-8522, Japan

Received: May 6, 2010; Revised Manuscript Received: June 7, 2010

The proton at the 2 position of the cation ring in imidazolium-based ionic liquids (ILs) strongly interacts with anions; therefore, the methylation at this position (C(2) methylation) causes significant changes in the physicochemical properties of these liquids. We investigated the C(2) methylation effects on the phase behaviors and cation conformations of ILs by calorimetric and Raman spectroscopic measurements, focusing on the pairs of 1-butyl-3-methylimidazolium salt ($[C_4mim]X$) and 1-butyl-2,3-dimethylimidazolium salt ($[C_4C_1mim]X$), where X^- is Cl^-, Br^-, I^-, BF_4^-, and PF_6^-. The melting and freezing points of all pairs increased after the C(2) methylation, as reported previously, and the reason for the increase was the overcompensation of the ΔS_{trans} decrease for the ΔH_{trans} decrease. The C(2) methylation also affected the phase behaviors of the ILs. With Raman spectroscopic measurements, all cation conformations in crystalline phases were assigned to trans−trans (TT), gauche−trans (GT), or gauche′−trans (G′T) conformers of the butyl group. Except in $[C_4C_1mim]BF_4$, all crystal−crystal phase transitions of the present samples occurred accompanied by conformational changes among TT, GT, and G′T. For the gas states of $[C_4mim]^+$ and $[C_4C_1mim]^+$, DFT calculations showed that there were hardly any differences in the structures of the butyl group for each set of paired conformers or in the energetic orders among the conformers. On the other hand, the conformer adopted in the crystalline phase differed between $[C_4mim]X$ and $[C_4C_1mim]X$. In addition, the population of the conformers in the liquid state also differed in each pair. The data from higher frequency Raman spectra suggested that the difference in cation conformation in each pair, for the crystalline and liquid states, was due to the shift in the position of the anion relative to that of the cation. By C(2) methylation, the relative distance between the anion and cation decreased for Cl^-, Br^-, and I^- salts, but it increased for BF_4^- and PF_6^- salts.

Introduction

Ionic liquids (ILs), which are composed solely of ions, are salts with low melting points. ILs are well-known to have certain outstanding properties as solvents, such as extremely low volatility and flammability, unique solubility, and wide electrochemical window. Therefore, ILs have attracted much attention in recent years and are considered as potential replacement for traditional volatile organic solvents.[1−5]

Imidazolium-based ILs are the most typical and widely studied ones. It is well-known that a proton at the 2 position of an imidazolium ring interacts strongly with anions. Therefore, the proton at this position plays an important role in the physicochemical properties, the structure, and the dynamics of the IL. It is noted that the interaction between the proton and anions is generally regarded as hydrogen bonding.[6−9] However, whether the interactions are hydrogen bonding in the conventional sense is still an open question.[10] Methylation at the 2 position of an imidazolium ring (C(2) methylation) significantly alters the physicochemical properties of ILs because of the drastic change in the interactions, structures, and dynamics of the liquid. For example, the C(2) methylation generally induces an increase in the melting point,[11−16] thermal stability,[13,15,17−19] viscosity,[11,17,20−22] surface tension,[13,23] chemical stability,[17,24] electrochemical stability,[11,17] vaporization enthalpy,[25] heat capacity,[12,18] and amphiphilicity[26] and also induces a decrease in density,[11,17,18] conductivity,[11,13,16,17,21] polarity,[13,27] and liquid crystallinity.[28] It is also reported that the C(2) methylation affects chemical reactivity in the methylated ILs[29] and improves tribological properties.[30] On the other hand, methylation at the 4 or 5 position of the imidazolium ring does not seem to affect the physicochemical properties of the ILs greatly.[11] Therefore, detailed investigations of the C(2) methylation effects at the molecular level are required. Recently, some reports on the C(2) methylation effects of ion structures and interactions have been published.[31−36] For example, Hunt predicted by quantum chemical calculations that an increase in the melting points and viscosities from the C(2) methylation originated from the reduced entropy.[31] However, the C(2) methylation effects are still unclear because few systematic and comprehensive studies exist.

In this paper, we report the C(2) methylation effects of imidazolium-based ILs on their phase behaviors and cation conformations by investigating with calorimetry and Raman spectroscopy, comparing five pairs of ILs, each comprising a nonmethylated and a methylated IL. The ILs used in this study are simple and typical; namely, cations of 1-butyl-3-methylimidazolium ($[C_4mim]^+$) and 1-butyl-2,3-dimethylimidazolium ($[C_4C_1mim]^+$) and anions of Cl^-, Br^-, I^-, BF_4^-, and PF_6^-. Structures and numbering of the atoms for these samples are shown in Chart 1.

Experimental Section

1. Samples. $[C_4mim]X$ and $[C_4C_1mim]X$ (where X^- is Cl^-, Br^-, I^-, BF_4^-, and PF_6^-) were prepared by the following

* To whom correspondence should be addressed. Fax: +81-43-290-3939. E-mail: k.nishikawa@faculty.chiba-u.jp.

10.1021/jp104123v
Published on Web 06/24/2010

CHART 1: Structures of [C_4mim]X and [C_4C_1mim]X (where X^- is Cl^-, Br^-, I^-, BF_4^-, and PF_6^-) and Numbering of Atoms

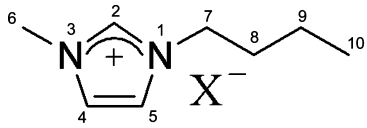

[C_4mim]X

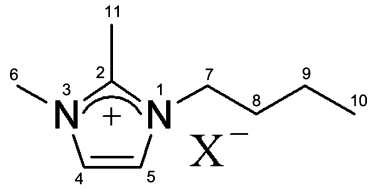

[C_4C_1mim]X

procedures. The ILs including halide anions were synthesized from 1-methylimidazole or 1,2-dimethylimidazole with halogenobutane. These ILs, except [C_4mim]I, were recrystallized several times to obtain colorless ILs. The ILs containing BF_4 or PF_6 anions were prepared by metathesis of the corresponding halides using $NaBF_4$ or $NaPF_6$. Then they were washed with distilled water several times until halide ions were not detected by $AgNO_3$ aqueous solution.

All the samples were characterized by ^{1}H NMR (JEOL JNM-LA500). In addition, the ILs containing BF_4 and PF_6 anions were also characterized by elemental analysis (Perkin-Elmer 2400), the results of which are summarized in the Supporting Information. All samples were dried at ~333 K under vacuum (10^{-3} Pa) over 24 h before use. All sample handling was performed in a N_2 atmosphere glovebox to avoid absorption of atmospheric moisture. The water content after completion of all preparations was below 150 ppm, except for [C_4mim]I (360 ppm), as measured by Karl Fischer titration (Mettler-Toledo model DL39 coulometer).

2. Measurements. Previously, we constructed an apparatus combining a commercially available Raman spectrometer and a laboratory-made calorimeter.[37] This is applicable as a Raman spectrometer equipped with a temperature controller with high stability as well as an apparatus for simultaneous measurement of Raman spectroscopy and calorimetry. We adopted a Raman spectrometer with an optical fiber (HoloLab 5000, Kaiser Optical Systems) and a GaAlAs diode laser (wavelength 785 nm). A spectrum in the range of 100−3450 cm^{-1} can be measured at once with a spectral resolution of 4 cm^{-1}. The maximum output power of the laser was 400 mW, and the diameter of the laser spot was ~80 μm. Curve fittings of Raman bands were performed by mixed Gaussian and Lorentzian functions. The laboratory-made calorimeter used here is a simpler type of our supersensitive DSC, the fundamental and original idea for which was previously reported.[38] These calorimeters adopt thermo modules as both heat-flow sensor and heat pump and enable us to perform calorimetric measurements with high sensitivity and temperature stability. The baseline stability and temperature of the present calorimeter were measured to be ~5 μW and ±0.001 K, respectively. Temperature can be scanned at very slow heating and cooling rates (minimum value, 0.5 mK/s).

3. DFT Calculations. DFT calculations were carried out using the Gaussian 03 program package.[39] Both full geometry optimizations and normal frequency analyses for the ions in the gas phase were performed using 6-311+G(d, p) basis sets based on the Becke's three-parameter hybrid method[40] with the LYP correlation (B3LYP).[41,42] No imaginary frequencies were produced by the optimized structures; this ensured the presence of a minimum. A scaling factor was not applied to the calculated frequency or to the thermal properties in the calculations.

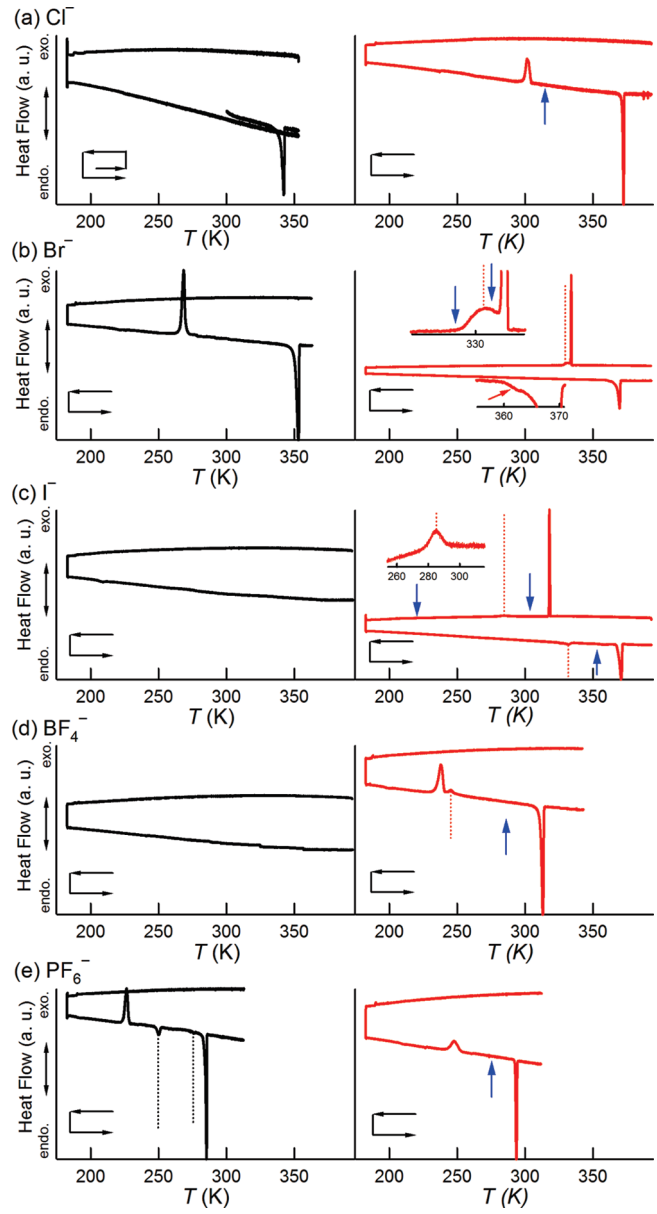

Figure 1. Calorimetric curves of [C_4mim]X (black curves) and [C_4C_1mim]X (red curves). (a) Cl^- salts, (b) Br^- salts, (c) I^- salts, (d) BF_4^- salts, and (e) PF_6^- salts. Dotted lines indicate crystal−crystal phase transitions. Temperature range is from 183 K to the temperature overmelting point, and scanning rate is 5 mK/s. The sequence of cooling and heating is demonstrated by the black arrows in each panel. Except for [C_4mim]Cl, all measurements started with sample cooling from the liquid state down to 183 K, followed by heating. [C_4mim]Cl melted first with heating from the crystalline state, and then followed by the same procedure as the other samples. The red arrow in [C_4C_1mim]Br indicates a crystal−crystal phase transition in the premelting region. The small peaks observed at ~190 K are experimental artifacts. The blue arrows demonstrate the measuring points of Raman scattering (see Figure 3).

Results and Discussion

1. Phase Behaviors Concerned with Melting and Crystallization. Figure 1 shows calorimetric curves of the ILs studied

TABLE 1: Thermodynamic Properties of [C_4mim]X and [C_4C_1mim]X and the Number of Crystal Phases Observed Here for the ILs[a]

	mp (K)	ΔH_{fusion} (kJ mol^{-1})	ΔS_{fusion} (J mol^{-1} K^{-1})	fp (K)	$\Delta H_{freezing}$ (kJ mol^{-1})	$\Delta S_{freezing}$ (J mol^{-1} K^{-1})	crystal phase number
[C_4mim]Cl	342.3	21	61.3				1
[C_4C_1mim]Cl	372.5	18.4	49.4	301.8	13.4	44.4	1
[C_4mim]Br	353	26.7	75.6	−268.5	18.3	68.2	1
[C_4C_1mim]Br	369.8	27.5	74.4	334	17.9	53.6	2
[C_4mim]I							
[C_4C_1mim]I	370.8	21.6	58.3	317.9	19	59.8	2
[C_4mim]BF_4							
[C_4C_1mim]BF_4	313.1	17.4	55.6	−238.1	7.2	30.2	2
[C_4mim]PF_6	285.3	13.3	46.6	−226.4	7.1	31.4	3
[C_4C_1mim]PF_6	293.6	9	30.7	−247.9	5.2	21	1

[a] The melting and freezing points are defined as the peak-top values of the calorimetric curves.

here: left panels for [C_4mim]X and right panels for [C_4C_1mim]X. The measured temperature range was from 183 K to the temperature exceeding the individual melting point. To divide overlaid peaks, the scanning rate was set to 5 mK/s, which is much lower than the conventional rate. The broken lines indicate crystal−crystal transitions.

Investigating the calorimetric curves, it is noted that there were significant differences in the melting and crystallization behaviors between [C_4mim]X and [C_4C_1mim]X. All [C_4C_1mim]$^+$-based ILs showed freezing and melting points, whereas those for [C_4mim]I and [C_4mim]BF_4 were not observed. As for [C_4mim]Cl, although crystallization from the supercooled liquid was reported,[43] the freezing point was not observed here. These results indicate that the [C_4mim]$^+$-based ILs are generally hard to crystallize as compared with the [C_4C_1mim]$^+$-based ILs.

All freezing and melting points of Cl^-, Br^-, and PF_6^- salts (except the freezing point of [C_4mim]Cl, because this freezing point was not observed) increased following the C(2) methylation, which is consistent with previous reports.[11−16] These phase-transition temperatures are described by

$$T_{trans} = \Delta H_{trans}/\Delta S_{trans} \quad (1)$$

where ΔH_{trans} and ΔS_{trans} are transition enthalpy and entropy, respectively. A summary of the thermodynamic properties of the present ILs, including ΔS_{trans} calculated from eq 1, are listed in Table 1. By the C(2) methylation, all of the fusion and freezing enthalpies, ΔH_{fusion} and $\Delta H_{freezing}$, decreased, except ΔH_{fusion} of Br^- salts. This decrease was considered to be due to a decrease in either the interaction energy between a cation and an anion or the lattice energy by the C(2) methylation, as reported earlier.[31,33,44] The exceptional slight increase of ΔH_{fusion} in Br^- salts was due to a crystal−crystal transition of [C_4C_1mim]Br during premelting (see the red arrow in the inset of Figure 1b). This small endothermic peak observed during the heating process corresponds to the broad exothermic peak observed in the cooling process just after crystallization. These traces suggest that sluggish phase transitions occurred; we will be investigating this in detail. On the other hand, all fusion and freezing entropies, ΔS_{fusion} and $\Delta S_{freezing}$, decrease followed by the C(2) methylation. This entropy decrease causes increasing melting and freezing points, that is, the decrease in ΔS_{trans} overcompensates for the decrease in ΔH_{trans}. This finding is consistent with the results obtained from the quantum chemical calculations by Hunt,[31] who reported that the ΔS_{trans} decrease was caused by the inhibition of the butyl group rotation and the decrease of stable ion pairs by the C(2) methylation.[31]

TABLE 2: Reported Melting Point, ΔH_{fusion} and ΔS_{fusion}[a]

	mp (K)/ΔH_{fusion} (kJ mol^{-1})/ ΔS_{fusion} (J mol^{-1} K^{-1})
[C_4mim]Cl	326.57/10.31/−,[12] 341.95/14.057/-,[77] 330/14.5/-,[43] 341/25.86/77.1[78]
[C_4C_1mim]Cl	365.89/14.41/−,[12] 370.0/18.5/-,[15] 373.0/14.53/-[79]
[C_4mim]Br	347.5/16.3/-,[80] 347.5/23.6/-,[43] 351.35/22.88/65.12[81]
[C_4C_1mim]Br	349.66/15.62/-,[12] 365.9/20.2/-[15]
[C_4mim]I	270/−/−,[55] 201/−/−[82]
[C_4C_1mim]I	
[C_4mim]BF_4	192/−/−[82]
[C_4C_1mim]BF_4	267.3/10.0/-[15]
[C_4mim]PF_6	281.0/13.2/-,[15] 280.03/19.91/-,[46] 282/12/-,[47] 276.43/9.21/-,[83] 283.51/19.60/-[84]
[C_4C_1mim]PF_6	314.9/17.09/-[79]

[a] Only melting points were reported for [C_4mim]I and [C_4mim]BF_4.

Bis((trifluoromethyl)sulfonyl)amide anion (Tf_2N^-) is one of the most typical ions in ILs, and it is noted that the trend of melting points for Tf_2N^- is different from that obtained here; namely, the melting points of [C_4mim]Tf_2N and [C_4C_1mim]Tf_2N are ∼270[45] and 260 K,[17] respectively. This seems to be due to the flexibility of the Tf_2N^- anion. The flexibility can increase ΔS_{fusion}; hence, the difference in ΔS_{fusion} between [C_4mim]Tf_2N and [C_4C_1mim]Tf_2N will become smaller as compared with that of the ILs studied here. Then, a decrease in ΔH_{fusion} from the C(2) methylation leads to a lower melting point. The relatively high ΔS_{fusion} values (77.3−91.4 J mol^{-1} K^{-1})[45−49] of [C_4mim]Tf_2N support this interpretation (no ΔS_{fusion} values of [C_4C_1mim]Tf_2N were reported).

The thermodynamic properties obtained here were compared with those previously reported. There are large differences in the values due to the differences in purities or experimental and analytical methods. Table 2 summarizes the reported thermodynamic values of the ILs as a reference.

2. Cation Conformation. As shown in Figure 1, some ILs studied here exhibited crystal−crystal phase transitions. These phenomena will be discussed in this section because they are related to the conformation of the cations.

2.1. Gas States. First, we performed the DFT calculations to reveal structural differences between [C_4mim]$^+$ and [C_4C_1mim]$^+$. The structures and interaction energies of both cations in the gas phase were previously reported in detail by Hunt.[31] Here, we focus on the cation conformations for the two ions. The number of stable cation conformations was found to be 11 for [C_4mim]$^+$ and 9 for [C_4C_1mim]$^+$ at the B3LYP/6-311+G(d,p) level. The difference in these conformations in each IL was caused by the rotation of the butyl group. Although these numbers depend on the computational level, the fact that the number in [C_4mim]$^+$ is greater than that in [C_4C_1mim]$^+$ is

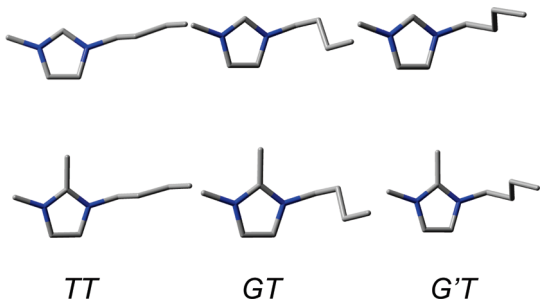

Figure 2. Structures of TT, GT, and G′T conformers for both $[C_4mim]^+$ (upper) and $[C_4C_1mim]^+$ (lower).

consistent with the ΔS_{trans} values obtained from the calorimetric measurements. For each conformer, the cation-conformational structure of $[C_4C_1mim]^+$ is almost the same as that of $[C_4mim]^+$, except for the small difference in the dihedral angle of the base of the butyl group (see Supporting Information Table 1S). The trend of the difference in energy (ΔE), enthalpy (ΔH), and Gibbs free energy (ΔG) in the cation conformations for $[C_4C_1mim]^+$ is similar to that for $[C_4mim]^+$ (Supporting Information Table 2S). These findings indicate that neither the structure nor the energy would be affected by the C(2) methylation in the gas phase.

2.2. Crystalline States. Crystal−crystal phase transitions were observed in some ILs, as shown in Figure 1, and their transition behaviors changed after the C(2) methylation. We measured Raman spectra to identify the cation-conformational structure for each crystal phase. As mentioned above, there are 9 or more possible conformations in each cation. Nevertheless, we focused on only three conformations for each $[C_4mim]^+$ and $[C_4C_1mim]^+$ in the crystal and liquid states by considering both the results from the single crystal structure analyses for the IL[16,50−57] and the energy differences in the conformations (Table 2S). The three conformers were the trans−trans (TT), gauche−trans (GT), and gauche′−trans (G′T), which are shown in Figure 2. It should be noted that other conformations may exist, especially in the liquid states—for example, a gauche−gauche conformer[58−60]—but they can be regarded as minor components.[59,60]

The cation conformations in the crystalline states for the $[C_4mim]^+$-based ILs except $[C_4mim]BF_4$ were revealed previously with X-ray single crystal analyses[50,51,53,55,56] or Raman spectroscopy.[61−63] The results for the ILs observed here agreed with previous Raman spectroscopic results. Therefore, assignments of cation conformation in the crystalline state were performed with Raman spectroscopy only for $[C_4C_1mim]X$ in this section. Figure 3 shows both obtained Raman spectra in each crystalline phase and calculated Raman bands of TT, GT, and G′T. The measuring points of the Raman spectra are denoted by blue arrows in Figure 1. Remarkable differences in the obtained spectra were observed in the range of 690−780 cm^{-1}. By comparing observed and calculated Raman spectra, the differences originated from the conformational isomerism due to the butyl rotation, as in the case of $[C_4mim]X$.[61−63] The crystal phase with a peak at ∼725 cm^{-1} was assigned to the crystal with the TT conformer, and the phase with two peaks at ∼708 and 725 cm^{-1} was assigned to the crystal with the GT or G′T conformer. The differences between GT and G′T appear in the intensity ratio of the Raman peak at 708 cm^{-1} against the peak at 725 cm^{-1} and in the spectral range of 450−550 cm^{-1}. The summary of conformation assignments of the cations for both $[C_4mim]X$ and $[C_4C_1mim]X$ are listed in Table 3 with the results from single-crystal analyses. All $[C_4C_1mim]^+$-based ILs have the crystalline phase with the TT conformer, but no crystalline phase with the G′T conformer was observed.

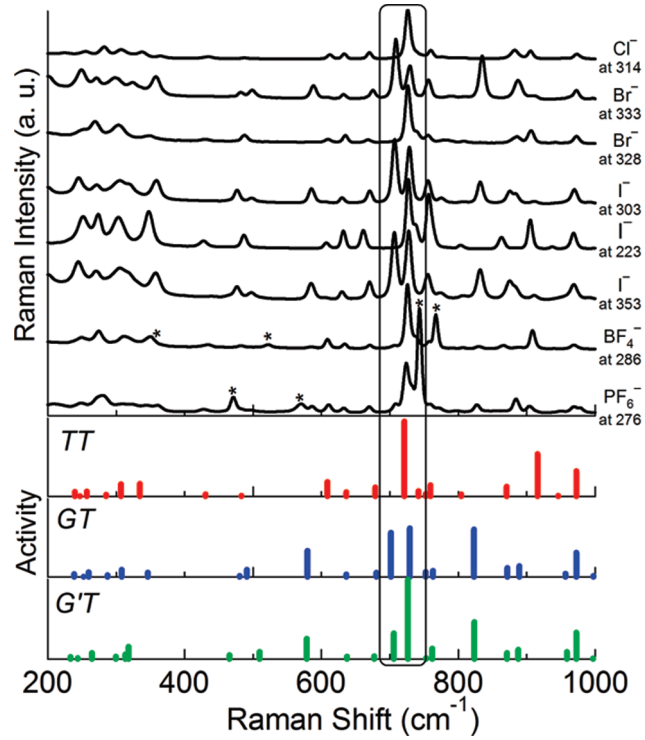

Figure 3. Observed Raman spectra of $[C_4C_1mim]X$ (black lines) for each crystalline phase and calculated Raman bands of TT (red), GT (blue), and G′T (green). Asterisks indicate anion bands. The measuring points of these Raman spectra are demonstrated by blue arrows in the calorimetric curves in Figure 1.

TABLE 3: Cation Conformations Observed Here in the Crystal Phases and Previously Reported in Single-Crystal Structure-Analysis Data

	observed cation conformation	reported cation conformation
$[C_4mim]Cl$	TT	TT, GT[50,51]
$[C_4C_1mim]Cl$	TT	TT, GT[52,54]
$[C_4mim]Br$	GT	GT[51]
$[C_4C_1mim]Br$	TT ↔ GT	GT[57]
$[C_4mim]I$		GT[55]
$[C_4C_1mim]I$	TT ↔ GT	TT[57]
$[C_4mim]BF_4$		
$[C_4C_1mim]BF_4$	TT	TT[16]
$[C_4mim]PF_6$	GT → TT → G′T	G′T[53,56]
$[C_4C_1mim]PF_6$	TT	GT[16]

Almost all crystal−crystal phase transitions for $[C_4C_1mim]X$ occurred accompanied by conformational changes, the trends of which were the same as that of $[C_4mim]PF_6$.[63] However, it is noted that the phase transition in $[C_4C_1mim]BF_4$ occurred without an accompanying conformational change. We named the two crystalline phases crystal α and crystal β, in order of increasing temperature. Figure 4a shows Raman spectra of $[C_4C_1mim]BF_4$ before and after the transition, that is, crystal α and crystal β, respectively. Figure 4b shows the calorimetric curve of $[C_4C_1mim]BF_4$ around the transition. To highlight the crystal−crystal phase transition in the calorimetric measurement, heating began from the crystalline state at 207 K, obtained by cooling immediately after crystallization at 238 K, that is, by cooling of crystal α. In this heating process, the large peak due to the crystallization from supercooled liquid to crystal α did not appear. Although a broad peak was observed near 253 K in the calorimetric curve, which agrees with the peak as shown in Figure 1, the Raman spectrum did not change after the phase

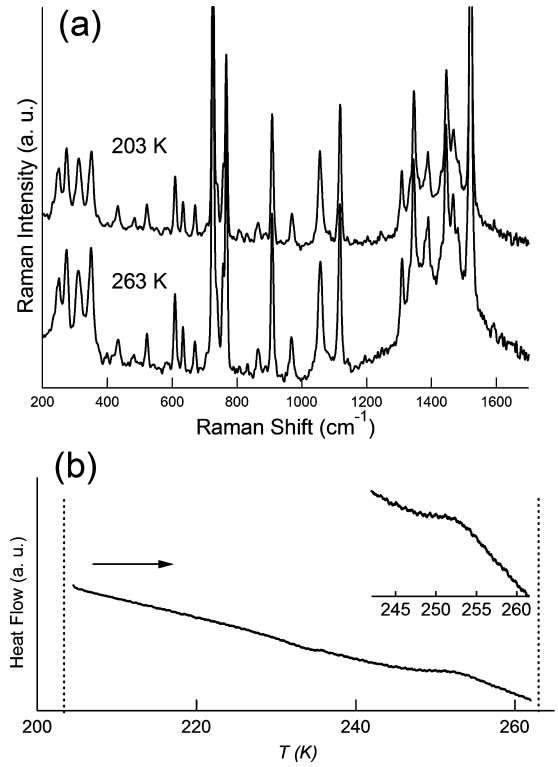

Figure 4. (a) Raman spectra of $[C_4C_1mim]BF_4$ before and after a crystal−crystal transition; (b) a calorimetric curve of $[C_4C_1mim]BF_4$ for the crystal−crystal transition. Scanning rate was set to 20 mK/s. Dotted lines indicate temperatures where the Raman spectra were measured.

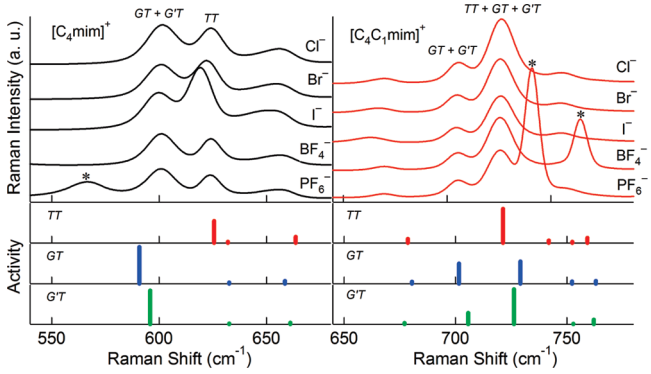

Figure 5. Observed Raman spectra of $[C_4mim]X$ (black lines) and $[C_4C_1mim]X$ (red lines) in the liquid state at 373 K. Calculated Raman bands are shown as reference. Asterisks indicate anion bands.

transition. Such a transition was also observed in Tf_2N-based ILs,[64] and this unique transition is under investigation.

2.3. Liquid States. Figure 5 shows Raman spectra of both $[C_4mim]X$ and $[C_4C_1mim]X$ in the liquid states at 373 K in the spectral range where marker bands for TT, GT, and G′T were observed. This figure indicates that the liquid state consists of a mixture of conformers, and the population ratio of the conformers seemed to vary depending on anion species, especially in $[C_4mim]X$. Figure 6 shows the temperature dependence of the intensity ratios of the Raman bands that were assigned as the marker bands for the conformational isomers. I_{TT} and $I_{GT+G'T}$ of $[C_4mim]X$ are the intensities for the TT conformer band at ∼622 cm^{-1} and for the mixed GT and G′T conformers band at ∼601 cm^{-1}, respectively. $I_{TT+GT+G'T}$ and $I_{GT+G'T}$ of $[C_4C_1mim]X$ are the intensities for the mixed TT, GT, and G′T conformers band at ∼726 cm^{-1} and for the mixed GT and G′T conformers band at ∼705 cm^{-1}, respectively. This figure qualitatively shows the relative stability of the TT conformer in the liquid state. It is noted that the quantitative analysis was difficult because there were many conformers in the liquid states, and the marker Raman bands of some conformers overlapped with others.

The results indicate that the population ratios of most ILs increase with increasing temperature, which means that the TT conformer is not generally the most stable conformer in the liquid state for both $[C_4mim]X$ and $[C_4C_1mim]X$. This is not consistent with the results from the DFT calculations. However, Tsuzuki et al. reported that the GT conformer becomes the most stable conformer through ion pair formation,[65] which supports the findings obtained here in the liquid states. The relative ratio in Figure 6 shows anion dependence. In $[C_4mim]X$, the trend of relative population of the TT conformer is in $BF_4^- \approx PF_6^- \approx Cl^- < Br^- < I^-$, which agrees with the results reported by Hamaguchi et al.[66] On the other hand, the trend in $[C_4C_1mim]X$ is different from that in $[C_4mim]X$; that is, $PF_6^- < BF_4^- \approx Br^- \approx Cl^- \approx I^-$. This difference between $[C_4mim]X$ and $[C_4C_1mim]X$ seems to be caused by the presence of anions and may relate to the differences in the phase transitions and cation conformations in the crystalline states.

3. Anion Position. As mentioned above, the different trends in adoption of the conformers in $[C_4mim]X$ and $[C_4C_1mim]X$ were observed in both crystalline and liquid states, and DFT calculation, for gas phases of the cations, did not reveal distinct differences in the structures of the butyl group for the paired conformers or in the energetic order of the conformers. This was due to the influence of the anions. Therefore, we investigated the anion position relative to the cation by analyses of higher-frequency Raman spectra. The bands of C−H stretching modes were observed in a frequency region higher than 2900 cm^{-1}, and it is known that these bands shift depending on the position of the anion relative to that of the cation of imidazolium-based ILs.[8,33,58,60,67−74]

Figure 7 shows calculated Raman spectra of $[C_4mim]^+$ and $[C_4C_1mim]^+$ in the high-frequency region. In the range of 2950−3200 cm^{-1}, which includes the C−H stretching modes of butyl and methyl groups, the spectra were different for two cations because of the presence of the methyl group at the 2 position of $[C_4C_1mim]^+$. On the other hand, the spectra were similar in the region 3240−3320 cm^{-1}, which includes the C−H stretching modes of the imidazolium ring. We note that our results of DFT calculations showed that spectra in this region were scarcely affected by the conformational change of the cations (data are not shown). The bands at the highest frequency, ∼3290 cm^{-1}, were assigned to the symmetric stretching modes of C−H at the 4 and 5 positions of the imidazolium ring (C(4)−H/C(5)−H). Therefore, anion positions relative to a proton at the 4 or 5 position of the imidazolium ring can be estimated by comparing these bands. It should be noted that the higher-frequency region of vibrational spectra would include the bands originating from Fermi resonance[73,75] or ion pair formation.[68]

Figure 8 shows higher-frequency Raman spectra of $[C_4mim]X$ and $[C_4C_1mim]X$ in the crystalline states. Here, we focused on Cl^-, Br^-, and PF_6^- salts because $[C_4mim]I$ and $[C_4mim]BF_4$ did not crystallize in our experiments. Changing the anion caused the Raman spectra for each series to differ. It is important to mention here that Raman spectra in the region 3000−3200 cm^{-1}, which includes the C−H stretching modes of the imidazolium ring, significantly change due to C(2) methylation. This suggests that the anion position relative to the cation changes with the C(2) methylation. For Cl^- salts, the band of

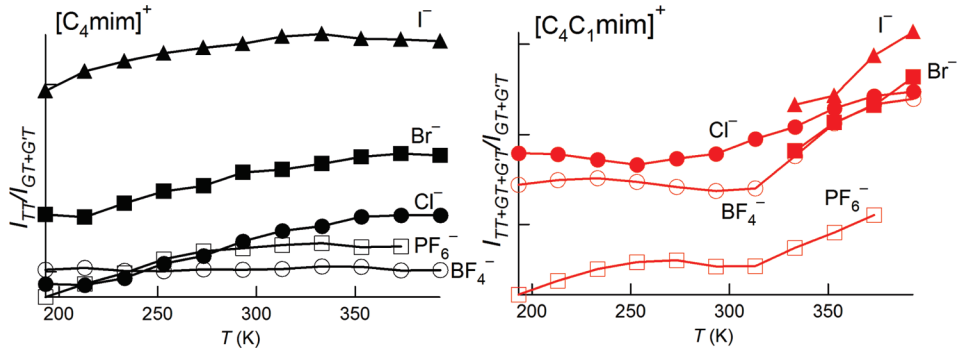

Figure 6. Temperature dependences of intensity ratios of Raman bands for $[C_4mim]X$ (black lines) and $[C_4C_1mim]X$ (red lines). I_{TT} and $I_{GT+G'T}$ of $[C_4mim]X$ are the integrated band intensities at ~622 and 601 cm^{-1}, respectively. $I_{TT+GT+G'T}$ and $I_{GT+G'T}$ of $[C_4C_1mim]X$ are the integrated band intensities at ~726 and 705 cm^{-1}, respectively. Solid circle, square, and triangle represent Cl^-, Br^-, and I^- salts, respectively. Open circle and square represent BF_4^- and PF_6^- salts, respectively.

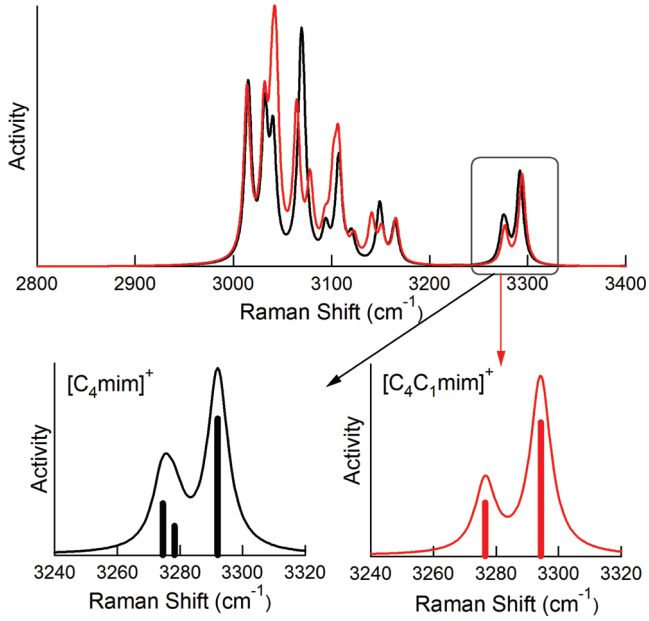

Figure 7. Calculated Raman spectra of $[C_4mim]^+$ (black line) and $[C_4C_1mim]^+$ (red line) in the higher-frequency region. In $[C_4mim]^+$, the bands at 3275, 3278, and 3292 cm^{-1} are assigned to C(4)−H/C(5)−H asymmetric stretching, C(2)−H stretching, and C(4)−H/C(5)−H symmetric stretching modes, respectively. In $[C_4C_1mim]^+$, the bands at 3277 and 3294 cm^{-1} are assigned to C(4)−H/C(5)−H asymmetric and symmetric stretching modes, respectively.

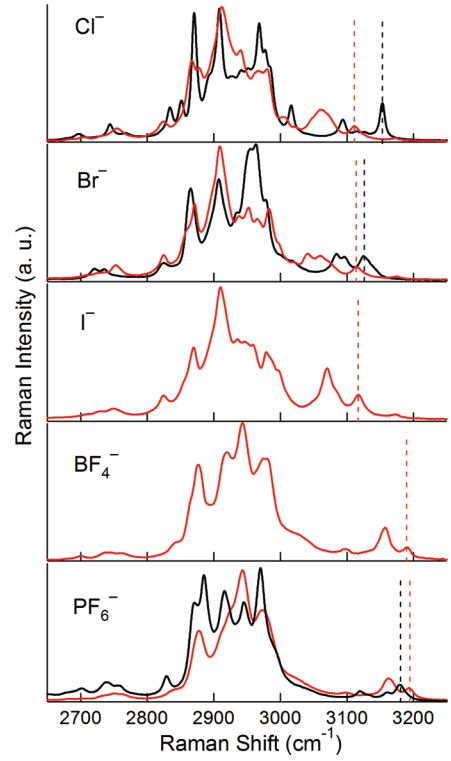

Figure 8. Observed higher-frequency Raman spectra of $[C_4mim]X$ (black lines) and $[C_4C_1mim]X$ (red lines) in the crystalline states. $[C_4mim]PF_6$ at 263 K, $[C_4C_1mim]I$ at 353 K, $[C_4C_1mim]PF_6$ at 273 K, and all the other ILs at 293 K. Dotted lines indicate the bands assigned to the C(4)−H/C(5)−H symmetric stretching mode.

$[C_4mim]Cl$ at 3153.2 cm^{-1}, marked by a black broken line, was assigned to the C(4)−H/C(5)−H symmetric stretching mode, and the band for $[C_4C_1mim]Cl$ shifted to a lower frequency of 3112.5 cm^{-1} (the band marked by a red broken line). This frequency shift corresponds to the results of single crystal structure analyses showing that the C(4)−H or the C(5)−H···Cl^- distance becomes shorter due to the C(2) methylation (reduction of 2.882[50] or 2.918 Å[51] for $[C_4mim]Cl$ to 2.663 or 2.793 Å for $[C_4C_1mim]Cl$[52]). As a result, the origin of the lower frequency shift due to the C(2) methylation will be the closer position of Cl^- to the protons at the 4 and 5 positions of the cation ring. Strong interaction between Cl^- and the protons at the 4 and 5 positions of the ring was also reported for 1-ethyl-2,3-dimethylimidazolium chloride.[76] The same trend was found in the case of Br^- salts; namely, the C(2) methylation caused the peak shift to the lower-frequency peak (from 3124.5 or 3135.1 cm^{-1} to 3115.5 cm^{-1}), and the distance became shorter (longer distances than the sum of van der Waals radii (3.050 Å) for $[C_4mim]Br$[51] to 2.733 Å and 2.821 Å for $[C_4C_1mim]Br$[57]). However, the opposite was true in the case of PF_6^- salts; namely, the C(2) methylation caused the Raman band to shift higher (3180.0 to 3194.2 cm^{-1}), and the average distance of C(4)−H/C(5)−H···F increased (2.434 and 2.563 Å[56] or 2.448, 2.590, and 2.669 Å[53] for $[C_4mim]PF_6$ to 2.479, 2.649, and 2.669 Å[16] for $[C_4C_1mim]PF_6$). In the case of PF_6^-salts, it should be noted that different conformational structures of the cation were compared here: specifically, the GT conformer for $[C_4C_1mim]$-PF_6[16] and the G′T conformer for $[C_4mim]PF_6$.[53,56] Raman spectra of $[C_4C_1mim]I$ and $[C_4C_1mim]BF_4$ in this region were similar to those of $[C_4C_1mim]Br$ (or $[C_4C_1mim]Cl$) and $[C_4C_1mim]PF_6$, respectively.

Figure 9 shows the experimental results for the liquid states. The trends of spectra in the region 2800−3250 cm^{-1} were divided into two groups: Cl^-, Br^-, and I^- salts and BF_4^- and PF_6^- salts. With the C(2) methylation, all spectra changed in the region 3000−3250 cm^{-1}, where C−H stretching modes of the imidazolium ring were included. For the Raman band

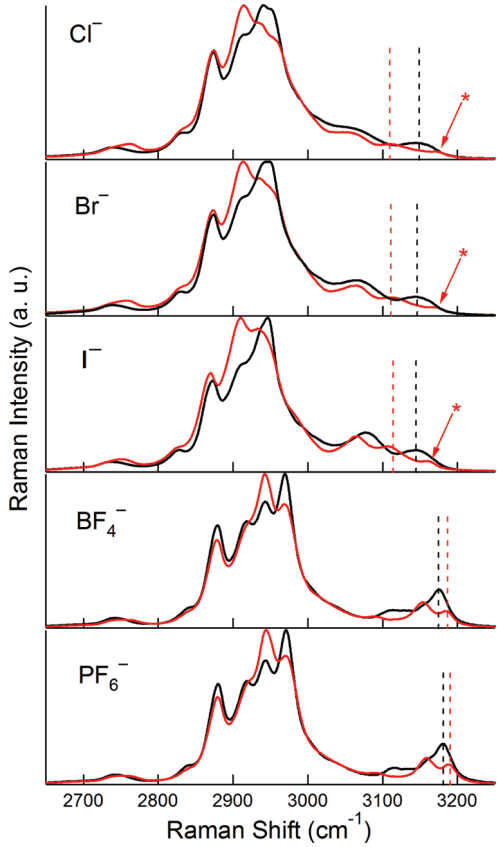

Figure 9. Observed higher-frequency Raman spectra of $[C_4mim]X$ (black lines) and $[C_4C_1mim]X$ (red lines) in the liquid states at 373 K. Dotted lines indicate the bands assigned to the C(4)−H/C(5)−H symmetric stretching mode, and asterisks indicate the small bands that are not assigned.

assigned to the C(4)−H/C(5)−H symmetric stretching mode, the bands of $[C_4mim]Cl$, $[C_4mim]Br$, and $[C_4mim]I$ shifted lower due to the C(2) methylation, whereas the bands of $[C_4mim]BF_4$ and $[C_4mim]PF_6$ shifted higher. This finding indicates that anion positions in $[C_4C_1mim]Cl$, -Br, and -I are closer to the proton at the 4 or 5 position than those in $[C_4mim]Cl$, -Br, and -I, but the opposite is true in the case of BF_4^- and PF_6^- salts. These results are similar to those obtained in the crystalline states. It is noted that the small bands at 3160 cm^{-1} in the liquid state for $[C_4C_1mim]Cl$, -Br, and -I (asterisks in Figure 9) could not be assigned; they were also observed as very small bands in the crystalline states.

In summary, the anion positions relative to the cations changed with the C(2) methylation in both the crystalline and liquid states. It is suggested that the anion position change is one of the main reasons for the difference in conformational structure between $[C_4mim]X$ and $[C_4C_1mim]X$. The Raman band positions assigned to the C(4)−H/C(5)−H symmetric stretching mode are summarized in Supporting Information Table 3S.

Conclusion

We have comprehensively investigated the C(2) methylation effects of imidazolium-based ILs on phase behaviors and cation conformations with calorimetry and Raman spectroscopy, focusing on pairs of $[C_4mim]X$ and $[C_4C_1mim]X$, where X^- is Cl^-, Br^-, I^-, BF_4^-, and PF_6^-. All the melting and freezing points of the ILs studied here increased with the C(2) methylation. The reason for the increase was the overcompensation of the ΔS_{trans} decrease for the ΔH_{trans} decrease. This experimental finding is consistent with the previous results obtained from quantum chemical calculations. Different phase behaviors were observed between $[C_4C_1mim]X$ and $[C_4mim]X$. Some ILs showed crystal−crystal phase transitions, and the cation conformations in each crystalline phase were determined by Raman spectroscopy. The cation conformations in crystalline phases were limited to trans−trans, gauche−trans, or gauche′−trans conformers of the butyl group. All crystal−crystal phase transitions occurred accompanied by cation-conformational changes, except in the case of $[C_4C_1mim]BF_4$. In both the crystalline and liquid states, the conformational difference was observed with the C(2) methylation, although for the gas state, there were no distinct differences in the structures of the butyl group for the paired conformers or in the energetic order of the conformers. The results from higher-frequency Raman spectra suggest that the differences in those states may be attributed to the change of the anion position relative to the cation following the C(2) methylation. As for Cl^-, Br^-, and I^- salts of $[C_4C_1mim]^+$, these anions were situated closer to the proton at the 4 or 5 positions of the ring than in the salts of $[C_4mim]^+$, whereas the opposite was true in the cases of BF_4^- and PF_6^- salts.

Acknowledgment. The present study was supported in part by the Ministry of Education, Culture, Sports, Science and Technology (MEXT) of Japan (No. 17073002, Grant-in-Aid for Scientific Research in Priority Area "Science of Ionic Liquids" (K.N.); No. 21245003, Grant-in-Aid for Scientific Research (A) (K.N.)). This work was also supported in part by the Global Center-of-Excellence Program "Advanced School for Organic Electronics" supported by MEXT (T.E.). We thank the Institute of Media and Information Technology of Chiba University for the provision of the computational facilities.

Supporting Information Available: Elemental analysis results and tables listing detailed computational results and experimental Raman band positions at the high-frequency region. This material is available free of charge via the Internet at http://pubs.acs.org.

References and Notes

(1) Wasserscheid, P.; Welton, T., Eds.; In *Ionic Liquids in Synthesis*; VCH-Wiley: Weinheim, Germany, 2003.
(2) Ohno, H., Ed.; In *Electrochemical Aspects of Ionic Liquids*; Wiley-Interscience: Hoboken, 2005.
(3) Welton, T. *Chem. Rev.* **1999**, *99*, 2071–2083.
(4) Wasserscheid, P.; Keim, W. *Angew. Chem., Int. Ed.* **2000**, *39*, 3773–3789.
(5) Sheldon, R. *Chem. Commun.* **2001**, 2399–2407.
(6) Dymek, C. J., Jr.; Grossie, D. A.; Fratini, A. V.; Adams, W. W. *J. Mol. Struct.* **1989**, *213*, 25–34.
(7) Dong, K.; Zhang, S.; Wang, D.; Yao, X. *J. Phys. Chem. A* **2006**, *110*, 9775–9782.
(8) Talaty, E. R.; Raja, S.; Storhaug, V. J.; Dölle, A.; Carper, W. R. *J. Phys. Chem. B* **2004**, *108*, 13177–13184.
(9) Hardacre, C.; Holbrey, J. D.; McMath, S. E. J.; Bowron, D. T.; Soper, A. K. *J. Chem. Phys.* **2003**, *118*, 273–278.
(10) Tsuzuki, S.; Tokuda, H.; Mikami, M. *Phys. Chem. Chem. Phys.* **2007**, *9*, 4780–4784.
(11) Bonhôte, P.; Dias, A. P.; Papageorgiou, N.; Kalyanasundaram, K.; Grätzel, M. *Inorg. Chem.* **1996**, *35*, 1168–1178.
(12) Zhu, J.; Bai, L.; Chen, B.; Fei, W. *Chem. Eng. J.* **2009**, *147*, 58–62.
(13) Yoshida, Y.; Baba, O.; Larriba, C.; Saito, G. *J. Phys. Chem. B* **2007**, *111*, 12204–12210.
(14) Larsen, A. S.; Holbrey, J. D.; Tham, F. S.; Reed, C. A. *J. Am. Chem. Soc.* **2000**, *122*, 7264–7272.
(15) Fox, D. M.; Awad, W. H.; Gilman, J. W.; Maupin, P. H.; De Long, H. C.; Trulove, P. C. *Green Chem.* **2003**, *5*, 724–727.
(16) Kölle, P.; Dronskowski, R. *Eur. J. Inorg. Chem.* **2004**, 2313–2320.
(17) Bazito, F. F. C.; Kawano, Y.; Torresi, R. M. *Electrochim. Acta* **2007**, *52*, 6427–6437.

(18) Fredlake, C. P.; Crosthwaite, J. M.; Hert, D. G.; Aki, S. N. V. K.; Brennecke, J. F. *J. Chem. Eng. Data* **2004**, *49*, 954–964.
(19) Awad, W. H.; Gilman, J. W.; Nyden, M.; Harris, R. H., Jr.; Sutto, T. E.; Callahan, J.; Trulove, P. C.; DeLong, H. C.; Fox, D. M. *Thermochim. Acta* **2004**, *409*, 3–11.
(20) Strehmel, V.; Laschewsky, A.; Wetzel, H.; Görnitz, E. *Macromolecules* **2006**, *39*, 923–930.
(21) Monteiro, M. J.; Bazito, F. F. C.; Siqueira, L. J. A.; Ribeiro, M. C. C.; Torresi, R. M. *J. Phys. Chem. B* **2008**, *112*, 2102–2109.
(22) Malham, I. B.; Turmine, M. *J. Chem. Thermodyn.* **2008**, *40*, 718–723.
(23) Freire, M. G.; Carvalho, P. J.; Fernandes, A. M.; Marrucho, I. M.; Queimada, A. J.; Coutinho, J. A. P. *J. Colloid Interface Sci.* **2007**, *314*, 621–630.
(24) Handy, S. T.; Okello, M. *J. Org. Chem.* **2005**, *70*, 1915–1918.
(25) Luo, H.; Baker, G. A.; Dai, S. *J. Phys. Chem. B* **2008**, *112*, 10077–10081.
(26) Kato, H.; Miki, K.; Mukai, T.; Nishikawa, K.; Koga, Y. *J. Phys. Chem. B* **2009**, *113*, 14754–14760.
(27) Lohse, P. W.; Bürsing, R.; Lenzer, T.; Oum, K. *J. Phys. Chem. B* **2008**, *112*, 3048–3057.
(28) Mukai, T.; Yoshio, M.; Kato, T.; Ohno, H. *Chem. Lett.* **2004**, *33*, 1630–1631.
(29) Itoh, T.; Nishimura, Y.; Ouchi, N.; Hayase, S. *J. Mol. Catal. B* **2003**, *26*, 41–45.
(30) Zhang, H.; Xia, Y.; Yao, M.; Jia, Z.; Liu, Z. *Tribol. Lett.* **2009**, *36*, 105–111.
(31) Hunt, P. A. *J. Phys. Chem. B* **2007**, *111*, 4844–4853.
(32) Fujii, K.; Mitsugi, T.; Takamuku, T.; Yamaguchi, T.; Umebayashi, Y.; Ishiguro, S. *Chem. Lett.* **2009**, *38*, 340–341.
(33) Fumino, K.; Wulf, A.; Ludwig, R. *Angew. Chem., Int. Ed.* **2008**, *47*, 8731–8734.
(34) Dahl, K.; Sando, G. M.; Fox, D. M.; Sutto, T. E.; Owrutsky, J. C. *J. Chem. Phys.* **2005**, *123*, 084504.
(35) Zahn, S.; Bruns, G.; Thar, J.; Kirchner, B. *Phys. Chem. Chem. Phys.* **2008**, *10*, 6921–6924.
(36) Mele, A.; Romanò, G.; Giannone, M.; Ragg, E.; Fronza, G.; Raos, G.; Marcon, V. *Angew. Chem., Int. Ed.* **2006**, *45*, 1123–1126.
(37) Endo, T.; Tozaki, K.; Masaki, T.; Nishikawa, K. *Jpn. J. Appl. Phys.* **2008**, *47*, 1775–1779.
(38) Wang, S.; Tozaki, K.; Hayashi, H.; Inaba, H. *J. Therm. Anal. Calorim.* **2005**, *79*, 605–613.
(39) Frisch, M. J.; Trucks, G. W.; Schlegel, H. B.; Scuseria, G. E.; Robb, M. A.; Cheeseman, J. R.; Montgomery, J. A., Jr.; Vreven, T.; Kudin, K. N.; Burant, J. C.; Millam, J. M.; Iyengar, S. S.; Tomasi, J.; Barone, V.; Mennucci, B.; Cossi, M.; Scalmani, G.; Rega, N.; Petersson, G. A.; Nakatsuji, H.; Hada, M.; Ehara, M.; Toyota, K.; Fukuda, R.; Hasegawa, J.; Ishida, M.; Nakajima, T.; Honda, Y.; Kitao, O.; Nakai, H.; Klene, M.; Li, X.; Knox, J. E.; Hratchian, H. P.; Cross, J. B.; Adamo, C.; Jaramillo, J.; Gomperts, R.; Stratmann, R. E.; Yazyev, O.; Austin, A. J.; Cammi, R.; Pomelli, C.; Ochterski, J. W.; Ayala, P. Y.; Morokuma, K.; Voth, G. A.; Salvador, P.; Dannenberg, J. J.; Zakrzewski, V. G.; Dapprich, S.; Daniels, A. D.; Strain, M. C.; Farkas, O.; Malick, D. K.; Rabuck, A. D.; Raghavachari, K.; Foresman, J. B.; Ortiz, J. V.; Cui, Q.; Baboul, A. G.; Clifford, S.; Cioslowski, J.; Stefanov, B. B.; Liu, G.; Liashenko, A.; Piskorz, P.; Komaromi, I.; Martin, R. L.; Fox, D. J.; Keith, T.; Al-Laham, M. A.; Peng, C. Y.; Nanayakkara, A.; Challacombe, M.; Gill, P. M. W.; Johnson, B.; Chen, W.; Wong, M. W.; Gonzalez, C.; Pople, J. A. *Gaussian 03*; Gaussian, Inc: Wallingford, CT, 2004.
(40) Becke, A. D. *J. Chem. Phys.* **1993**, *98*, 5648–5652.
(41) Lee, C.; Yang, W.; Parr, R. G. *Phys. Rev. B* **1988**, *37*, 785–789.
(42) Miehlich, B.; Savin, A.; Stoll, H.; Preuss, H. *Chem. Phys. Lett.* **1989**, *157*, 200–206.
(43) Nishikawa, K.; Wang, S.; Katayanagi, H.; Hayashi, S.; Hamaguchi, H.; Koga, Y.; Tozaki, K. *J. Phys. Chem. B* **2007**, *111*, 4894–4900.
(44) Tsuzuki, S.; Tokuda, H.; Hayamizu, K.; Watanabe, M. *J. Phys. Chem. B* **2005**, *109*, 16474–16481.
(45) Tokuda, H.; Hayamizu, K.; Ishii, K.; Susan, M. A. B. H.; Watanabe, M. *J. Phys. Chem. B* **2005**, *109*, 6103–6110.
(46) Troncoso, J.; Cerdeiriña, C. A.; Sanmamed, Y. A.; Romaní, L.; Rebelo, L. P. N. *J. Chem. Eng. Data* **2006**, *51*, 1856–1859.
(47) Jin, H.; O'Hare, B.; Dong, J.; Arzhantsev, S.; Baker, G. A.; Wishart, J. F.; Benesi, A. J.; Maroncelli, M. *J. Phys. Chem. B* **2008**, *112*, 81–92.
(48) Blokhin, A. V.; Paulechka, Y. U.; Strechan, A. A.; Kabo, G. J. *J. Phys. Chem. B* **2008**, *112*, 4357–4364.
(49) Shimizu, Y.; Ohte, Y.; Yamamura, Y.; Saito, K. *Chem. Phys. Lett.* **2009**, *470*, 295–299.
(50) Saha, S.; Hayashi, S.; Kobayashi, A.; Hamaguchi, H. *Chem. Lett.* **2003**, *32*, 740–741.
(51) Holbrey, J. D.; Reichert, W. M.; Nieuwenhuyzen, M.; Johnston, S.; Seddon, K. R.; Rogers, R. D. *Chem. Commun.* **2003**, 1636–1637.
(52) Kölle, P.; Dronskowski, R. *Inorg. Chem.* **2004**, *43*, 2803–2809.
(53) Choudhury, A. R.; Winterton, N.; Steiner, A.; Cooper, A. I.; Johnson, K. A. *J. Am. Chem. Soc.* **2005**, *127*, 16792–16793.
(54) Andre, M.; Loidl, J.; Laus, G.; Schottenberger, H.; Bentivoglio, G.; Wurst, K.; Ongania, K. H. *Anal. Chem.* **2005**, *77*, 702–705.
(55) Nakakoshi, M.; Shiro, M.; Fujimoto, T.; Machinami, T.; Seki, H.; Tashiro, M.; Nishikawa, K. *Chem. Lett.* **2006**, *35*, 1400–1401.
(56) Dibrov, S. M.; Kochi, J. K. *Acta Crystallogr.* **2006**, *C62*, o19–o21.
(57) Kutuniva, J.; Oilunkaniemi, R.; Laitinen, R. S.; Asikkala, J.; Kärkkäinen, J.; Lajunen, M. K. *Z. Naturforsch.* **2007**, *62b*, 868–870.
(58) Katsyuba, S. A.; Zvereva, E. E.; Vidiš, A.; Dyson, P. J. *J. Phys. Chem. A* **2007**, *111*, 352–370.
(59) Jayaraman, S.; Maginn, E. J. *J. Chem. Phys.* **2007**, *127*, 214504.
(60) Holomb, R.; Martinelli, A.; Albinsson, I.; Lassègues, J. C.; Johansson, P.; Jacobsson, P. *J. Raman Spectrosc.* **2008**, *39*, 793–805.
(61) Hayashi, S.; Ozawa, R.; Hamaguchi, H. *Chem. Lett.* **2003**, *32*, 498–499.
(62) Ozawa, R.; Hayashi, S.; Saha, S.; Kobayashi, A.; Hamaguchi, H. *Chem. Lett.* **2003**, *32*, 948–949.
(63) Endo, T.; Kato, T.; Tozaki, K.; Nishikawa, K. *J. Phys. Chem. B* **2010**, *114*, 407–411.
(64) Henderson, W. A.; Trulove, P. C.; DeLong, H. C.; Young, V. G., Jr. *ECS Trans.* **2007**, *3*, 83–88.
(65) Tsuzuki, S.; Arai, A. A.; Nishikawa, K. *J. Phys. Chem. B* **2008**, *112*, 7739–7747.
(66) Hamaguchi, H.; Ozawa, R. *Adv. Chem. Phys.* **2005**, *131*, 85–104.
(67) Berg, R. W.; Deetlefs, M.; Seddon, K. R.; Shim, I.; Thompson, J. M. *J. Phys. Chem. B* **2005**, *109*, 19018–19025.
(68) Köddermann, T.; Wertz, C.; Heintz, A.; Ludwig, R. *ChemPhysChem* **2006**, *7*, 1944–1949.
(69) Chang, H. C.; Jiang, J. C.; Tsai, W. C.; Chen, G. C.; Lin, S. H. *J. Phys. Chem. B* **2006**, *110*, 3302–3307.
(70) Chang, H. C.; Jiang, J. C.; Su, J. C.; Chang, C. Y.; Lin, S. H. *J. Phys. Chem. A* **2007**, *111*, 9201–9206.
(71) Jeon, Y.; Sung, J.; Seo, C.; Lim, H.; Cheong, H.; Kang, M.; Moon, B.; Ouchi, Y.; Kim, D. *J. Phys. Chem. B* **2008**, *112*, 4735–4740.
(72) Jeon, Y.; Sung, J.; Kim, D.; Seo, C.; Cheong, H.; Ouchi, Y.; Ozawa, R.; Hamaguchi, H. *J. Phys. Chem. B* **2008**, *112*, 923–928.
(73) Lassègues, J. C.; Grondin, J.; Cavagnat, D.; Johansson, P. *J. Phys. Chem. A* **2009**, *113*, 6419–6421.
(74) Gao, Y.; Zhang, L.; Wang, Y.; Li, H. *J. Phys. Chem. B* **2010**, *114*, 2828–2833.
(75) Wulf, A.; Fumino, K.; Ludwig, R. *J. Phys. Chem. A* **2010**, *114*, 685–686.
(76) Abdul-Sada, A. K.; Al-Juaid, S.; Greenway, A. M.; Hitchcock, P. B.; Howells, M. J.; Seddon, K. R.; Welton, T. *Struct. Chem.* **1990**, *1*, 391–394.
(77) Domańska, U.; Bogel-Łukasik, E.; Bogel-Łukasik, R. *Chem.—Eur. J.* **2003**, *9*, 3033–3041.
(78) Yamamuro, O.; Minamimoto, Y.; Inamura, Y.; Hayashi, S.; Hamaguchi, H. *Chem. Phys. Lett.* **2006**, *423*, 371–375.
(79) Henderson, W. A.; Young, V. G., Jr.; Fox, D. M.; De Long, H. C.; Trulove, P. C. *Chem. Commun.* **2006**, 3708–3710.
(80) Turner, E. A.; Pye, C. C.; Singer, R. D. *J. Phys. Chem. A* **2003**, *107*, 2277–2288.
(81) Paulechka, Y. U.; Kabo, G. J.; Blokhin, A. V.; Shaplov, A. S.; Lozinskaya, E. I.; Vygodskii, Y. S. *J. Chem. Thermodyn.* **2007**, *39*, 158–166.
(82) Huddleston, J. G.; Visser, A. E.; Reichert, W. M.; Willauer, H. D.; Broker, G. A.; Rogers, R. D. *Green Chem.* **2001**, *3*, 156–164.
(83) Domańska, U.; Marciniak, A. *J. Chem. Eng. Data* **2003**, *48*, 451–456.
(84) Kabo, G. J.; Blokhin, A. V.; Paulechka, Y. U.; Kabo, A. G.; Shymanovich, M. P.; Magee, J. W. *J. Chem. Eng. Data* **2004**, *49*, 453–461.

JP104123V